ACS OMEGA

Open Access

http://pubs.acs.org/journal/acsodf

Article

Effects of Reduction Methods on the Performance of *Shewanella oneidensis* MR-1 Palladium/Carbon Catalyst for Oxygen Reduction Reaction

Xiaoting Deng,* Min Lao, Jingwen Huang, Pan Wang, Shaofeng Yin, and Yili Liang*

Cite This: *ACS Omega* 2023, 8, 47616−47622

Read Online

ACCESS | Metrics & More | Article Recommendations | Supporting Information

ABSTRACT: The influence of the reduction method on the morphology and performance of the catalyst still controversial. In this study, hydrogen, *Shewanella oneidensis* MR-1 (MR-1), MR-1 and hydrogen coreduction are used to reduce the palladium ions adsorbed by MR-1 to obtain Pd/C_{H_2}, Pd/C_M, and Pd/C_{H_2+M} catalyst, respectively. It is found that the palladium nanoparticles (Pd NPs) in Pd/C_{H_2+M} are the largest, while the Pd NPs in Pd/C_M are the smallest. This is due to the reduction of Pd NPs in Pd/C_{H_2+M} under anaerobic conditions to form smaller Pd NPs that will further aggregate and grow in H_2. In addition, Pd/C_M exhibited the best catalytic performance with a mass activity of 0.31 A mg^{-1}, better than that of Pd/C_{H_2} (0.06 A mg^{-1}) and Pd/C_{H_2+M} (0.13 A mg^{-1}). This study provides a meaningful reference for the selection of reduction methods in metal catalysts.

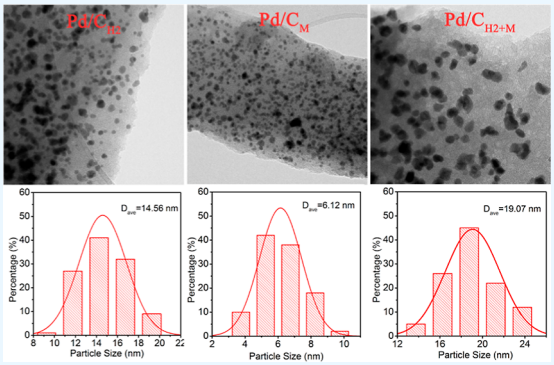

1. INTRODUCTION

Proton exchange membrane fuel cells (PEMFCs) are zero-emission, high-efficiency energy conversion devices. Platinum (Pt) is recognized as the most effective fuel cell cathode catalyst.[1] However, due to the low earth reserves and high price of Pt, researchers are working hard to find a new oxygen reduction catalyst. Among them, nanometal catalysts[2] and nonmetal catalysts[3] have been widely studied.

The process of preparing nanometal catalysts by the microbial method includes adsorption, carbonization, and reduction, using bacteria as carbon sources. Carbonization can improve the conductivity of the catalyst.[4] The purpose of the reduction is to reduce the adsorbed high-valence metal ions into zerovalent metals to play a catalytic role.[5] To improve the utilization of noble metals, one of the most ideal approaches is to reduce noble metal ions to the smallest possible nanoparticles or even single atoms.[6] However, studies have demonstrated that reactants induce atomic migration by coordinating with catalysts, thereby changing the structures of active sites and further enhancing their catalytic performance. H_2 reduction is the most common way of reduction. However, H_2 is considered to be a strong coordination reactant, which can increase the mobility of the surface atoms on the support. In addition, isolated single atoms tend to aggregate into nanoparticles under H_2, because traditional oxide or carbon supports cannot effectively stabilize metal single atoms under a H_2 atmosphere.[7] Therefore, the structural evolution of metals under H_2 reduction remains elusive.

Microorganisms can change the oxidation state of metals, which opens a new window for the biosynthesis of metal nanomaterials.[8] Most dissimilatory metal-reducing bacteria have electron transfer systems that can oxidize organic substances to obtain energy under anaerobic conditions.[9] *Shewanella oneidensis* MR-1 (MR-1) is a typical dissimilatory metal-reducing bacterium with strong resistance and adsorption ability to metals.[10] The electrons generated in the oxidation of organic matter are transferred to electron acceptors such as organic pollutants, metal oxides, and metal ions through different electron transfer mechanisms. Therefore, the redox system of microorganisms can be used to reduce metal ions. On the one hand, this makes the preparation process of nanometal catalysts more gentle, simple, and environmentally friendly; on the other hand, the regulation means of bioreduction are more diverse, and the particle size of the prepared nanometals is more controllable.[10b,11]

Received: August 6, 2023
Revised: November 16, 2023
Accepted: November 23, 2023
Published: December 1, 2023

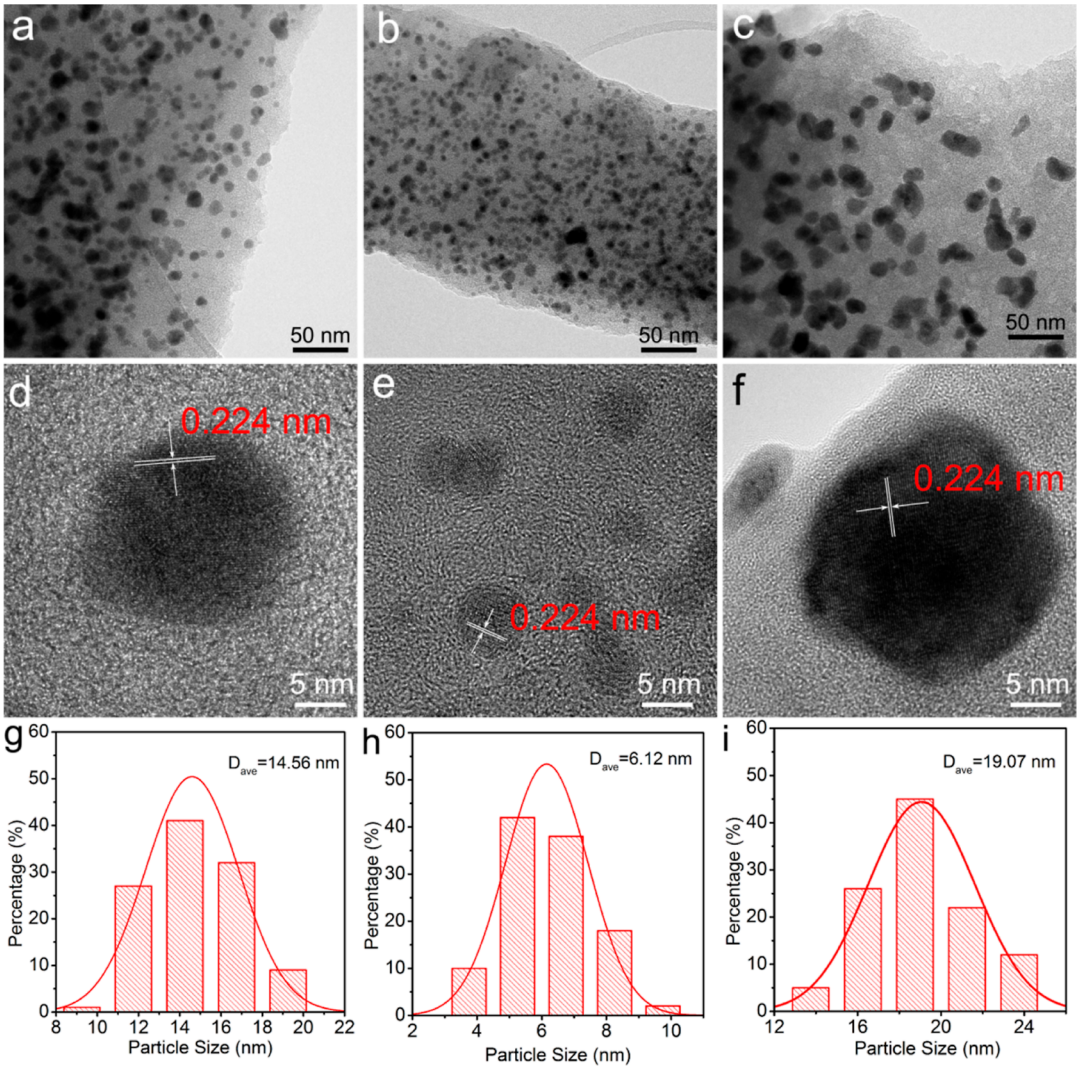

Figure 1. (a–c) TEM images, (d–f) HRTEM images, and (g–i) Pd size distribution of (a,d,g) Pd/C_{H_2}, (b,e,h) Pd/C_M, and (c,f,i) Pd/C_{H_2+M}, respectively.

However, there is a lack of work studying the effects of H_2 reduction and microbial reduction on nanometal catalysts. In this work, biopalladium carbon catalysts with different reduction modes were prepared using MR-1 as the carbon matrix, including H_2 reduction catalyst, MR-1 biological reduction catalyst, and MR-1 reduction plus H_2 reduction catalyst, and an in-depth analysis of the effect of the reduction modes on the catalyst structure and properties was performed.

2. EXPERIMENTAL PART

2.1. Chemicals. *S. oneidensis* MR-1 is self-cultured in the laboratory. Sodium tetrachloropalladate (Na_2PdCl_4), sodium formate, and Nafion (5 wt %) were purchased from Sinopharm Chemical Reagent Co., Ltd. All the reagents and solvents were used without further purification. Commercial 10% Pd/C was purchased from Johnson Matthey Company. DI water (18.2 MΩ·cm) was produced in our laboratory.

2.2. Synthesis of Catalysts. *2.2.1. Palladium Ion Adsorption.* The cultured *S. oneidensis* MR-1 was concentrated by centrifugation and washed with phosphoric acid buffer to be collected for later use. An appropriate amount of collected bacteria was dissolved in 25 mL of deionized water, and the concentration of bacterial culture (OD600 = 3.3) was controlled. 75 mL of sodium tetrachloropalladate solution with a concentration of 6.89 mmol/L was prepared. In addition, three parts of the abovementioned concentrated bacterial solution and sodium tetrachloropalladate solution were prepared, and the pH was adjusted to 3 with HCl. 5 mM sodium formate was added to two parts of the concentrated bacterial solution. The bacterial solution and sodium tetrachloropalladate solution were concentrated in an anaerobic incubator with N_2 to discharge O_2, and then the sodium tetrachloropalladate solution was added dropwise using a peristaltic pump. Another part of the bacterial solution and palladium solution was added dropwise in an open Erlenmeyer flask with a peristaltic pump. Three groups of samples were fully stirred with a magnetic stirrer while adding palladium; the dripping speed of the peristaltic pump was 0.5 mL/min; the rotating speed of the magnetic stirring was 400 rpm; and the reaction time was 24 h.

2.2.2. Carbonization and Reduction. The three samples completed by adsorption were freeze-dried in a vacuum overnight. After drying, the sample (named group A for adsorption in an aerobic environment and group B for adsorption in an anaerobic environment) was placed in a

https://doi.org/10.1021/acsomega.3c05765
ACS Omega 2023, 8, 47616–47622

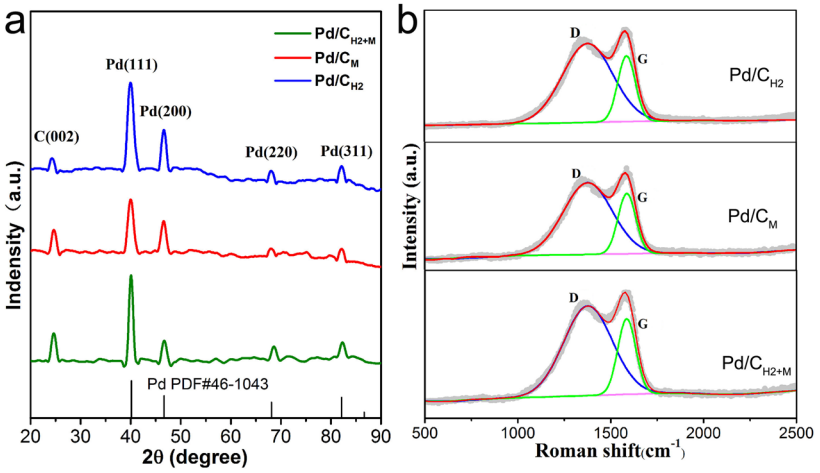

Figure 2. (a) XRD and (b) Raman spectra patterns of Pd/C_{H_2}, Pd/C_M, and Pd/C_{H_2+M}, respectively.

tube furnace. According to the reduction method, it can be divided into three groups. The specific operation steps were as follows: (a) group A samples were heated at a rate of 3 °C/min in an argon atmosphere to raise the temperature of the tube furnace to 800 °C for 3 h. Then the reduction process was conducted at 200 °C in a H_2/Ar (3:1) atmosphere for 2 h. The Pd ions in this sample were reduced by H_2, so they were named Pd/C_{H_2}; (b) samples of another group (group B samples) were heated at a rate of 3 °C/min in an argon atmosphere to raise the temperature of the tube furnace to 800 °C for 3 h. After cooling naturally, the argon gas was turned off and the sample was taken out, named Pd/C_M. (c) The group B samples were subjected to the same reduction treatment as were Pd/C_{H_2}, named Pd/C_{H_2+M}.

2.3. Characterization. Scanning electron microscopy (SEM) was conducted on MIRA4 LMH. Transmission electron microscopy (TEM) images were obtained by Titan G2 60e300. The X-ray diffraction (XRD) patterns were obtained on a Bruker Advance D8 X-ray diffractometer. The Raman spectrum was recorded on a Renishaw inVia spectrometer. X-ray photoelectron spectroscopy (XPS) was conducted on an ESCALAB 250 X-ray photoelectron spectrometer. The content of Pd was analyzed by inductively coupled plasma (ICP 7000 SERIES). The Pd contents of Pd/C_{H_2}, Pd/C_M, Pd/C_{H_2+M}, and Pd/C, measured by ICP, were 9.53, 6.63, 6.36, and 9.98%, respectively. Detailed procedures for electrochemical characterization are listed in the Supporting Information.

3. RESULTS AND DISCUSSION

3.1. Structural Characterization. The SEM images of Pd/C_{H_2}, Pd/C_M, and Pd/C_{H_2+M} are shown in Figure S1. The TEM images and particle size statistical images of the as-prepared catalyst samples are shown in Figure 1. Figure 1a–c shows that the nanoparticles are uniformly distributed on the carbon matrix. Figure 1 reveals that the interplanar spacing of the nanoparticles is 0.224 nm, corresponding to the (111) crystal plane of Pd. It can be seen that the palladium nanoparticles (Pd NPs) in Pd/C_{H_2+M} are the largest, followed by Pd/C_{H_2} and Pd/C_M, with the average particle size being 19.07, 14.56, and 6.12 nm, respectively. The main reason for the difference in the size of Pd NPs may be that H_2 is a strong

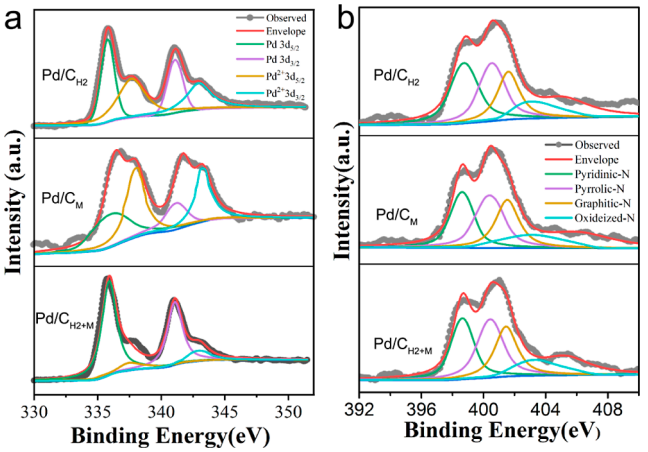

Figure 3. (a) Pd 3d spectra and (b) N 1S spectra of Pd/C_{H_2}, Pd/C_M and Pd/C_{H_2+M}.

coordination reactant, which can induce the migration of metal atoms on the carbon support and make the nucleated and aggregated Pd NPs continue to absorb more metal atoms around them and continue to grow, resulting in continuous growth of the particles.[7] Adsorption–reduction of Pd/C_M under anaerobic conditions was studied. The functional groups on the surface of MR-1 adsorb Pd(II) and directly reduce Pd(II) through its redox system, which avoids the migration and agglomeration of palladium atoms during the H_2 reduction process, so the formed particles are the smallest. However, the H_2 treatment group is adsorbed and reduced under aerobic conditions, and the electrons generated by microbial respiration and metabolism will be preferentially transferred to O_2 and cannot be reduced to Pd(II), so H_2 reduction treatment is required, and the formed Pd NPs are larger than those in Pd/C_M. Pd/C_{H_2+M} first forms smaller Pd NPs under anaerobic conditions, and the Pd NPs that have nucleated in the H_2 atmosphere will continue to gather the surrounding palladium, so the migration phenomenon is more serious than that of the H_2 reduction group, which leads to the largest Pd NPs in Pd/C_{H_2+M}.

Figure 2a shows the XRD spectrum of the as-prepared catalyst. All samples have diffraction peaks at 2θ = 24.6, 40.1, 46.65, 68.1, and 82.1°, corresponding to the (002) crystal

https://doi.org/10.1021/acsomega.3c05765
ACS Omega 2023, 8, 47616–47622

Table 1. Types and Content of Pd and N in Pd/C_{H_2}, Pd/C_M and Pd/C_{H_2+M}

samples	Pd(0)	Pd(II)	pyridinic-N	pyrrolic-N	graphitic N	oxidized-N
Pd/C_{H_2}	74.42	25.58	31.71	30.94	23.21	14.14
Pd/C_M	35.72	64.28	31.42	30.57	24.33	13.68
Pd/C_{H_2+M}	84.09	15.91	31.43	31.25	23.40	13.92

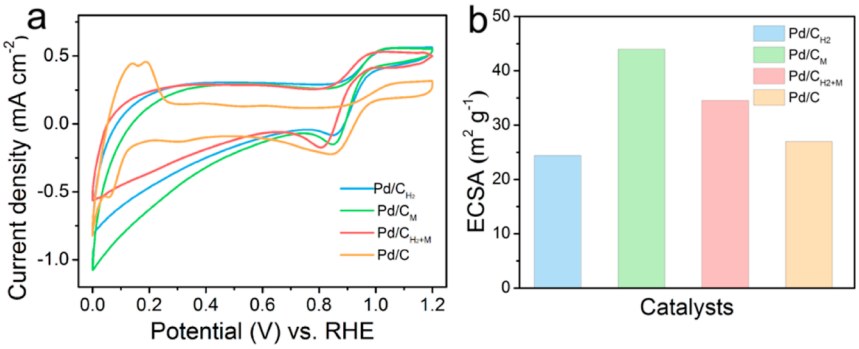

Figure 4. (a) CV and (b) ECSA of Pd/C_{H_2}, Pd/C_M, and Pd/C_{H_2+M} in a 0.1 M KOH solution with a potential scanning rate of 10 mV s^{-1}.

Table 2. Electrochemical Activity Indices of As-Prepared Catalysts

sample	E_{onset} (V)	ECSA (m^2 g^{-1})	MA (A mg^{-1})	SA (A m^{-2})	Pd (wt %)
Pd/C_{H_2}	0.999	24.39	0.06	0.25	9.53
Pd/C_M	0.103	43.97	0.31	0.71	6.63
Pd/C_{H_2+M}	0.967	34.53	0.13	0.37	6.36
commercial Pd/C	0.996	26.97	0.08	0.31	9.89

plane of C and (111), (200), (220), and (311) crystal planes of Pd, respectively.

The Raman results are shown in Figure 2b. The I_D/I_G ratios of Pd/C_{H_2}, Pd/C_M, and Pd/C_{H_2+M} are 1.20, 1.19, and 1.19, respectively. This shows that the degree of graphitization of the as-prepared catalysts is basically the same, because their carbon matrix is consistent.[12] Compared with the other two samples, Pd/C_M has not been reduced by H_2 at 200 °C, but this process has no effect on the degree of graphitization of the catalysts.

Figure 3 shows the Pd 3d spectrum and N 1S spectrum of the catalyst samples treated by different reduction methods, and the results are shown in Table 1. The spectra could be subdivided into four types of N: pyridinic N (398.5 eV), pyrrolic N (400.9 eV), graphite N (401.6 eV), and nitrogen oxide (403.4 eV).[13] As shown in Figure 3b, the proportions of different nitrogen species in Pd/C_{H_2}, Pd/C_M, and Pd/C_{H_2+M} are basically the same. This is because the three groups of catalysts used the same matrix. However, the Pd 3d spectrum shows that the proportion of palladium in different valence states is significantly different.[14] Pd(0) of Pd/C_{H_2+M} accounted for the highest proportion (84.09%), followed by Pd/C_{H_2} (74.42%), and Pd/C_M (47.39%) was the least. The largest proportion of Pd(0) in the Pd/C_{H_2+M} catalyst is due to its complete reduction. The reduction rate of Pd/C_M is obviously insufficient, which may be related to its reducing environment, such as palladium ion concentration, electron donor type and concentration, pH, bacterial concentration, etc.

3.2. Electrocatalytic Activity for ORR. The CV curves are shown in Figure 4a. Obviously, the oxygen reduction peaks of as-prepared catalysts can be seen in the CV curves, and the oxygen reduction peaks of Pd/C_{H_2}, Pd/C_M, and Pd/C_{H_2+M} are located at 0.851, 0.853, and 0.807 V, respectively. Among them, the oxygen reduction potentials of Pd/C_{H_2} and Pd/C_M are relatively close, and both are better than those of commercial Pd/C (0.84 V). But the oxygen reduction potential of Pd/C_{H_2+M} is the smallest. This indicates that the performance of the Pd/C_{H_2+M} catalyst after two reductions is poor, while the performance of the Pd/C_{H_2}, Pd/C_M catalysts is

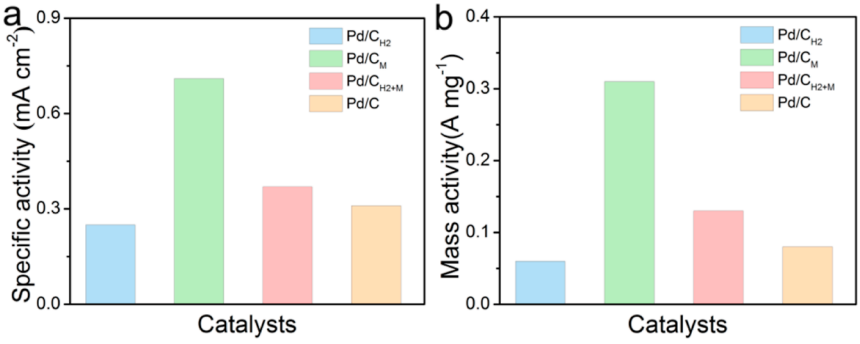

Figure 5. (a) SA and (b) MA of Pd/C_{H_2}, Pd/C_M, and Pd/C_{H_2+M}.

https://doi.org/10.1021/acsomega.3c05765
ACS Omega 2023, 8, 47616−47622

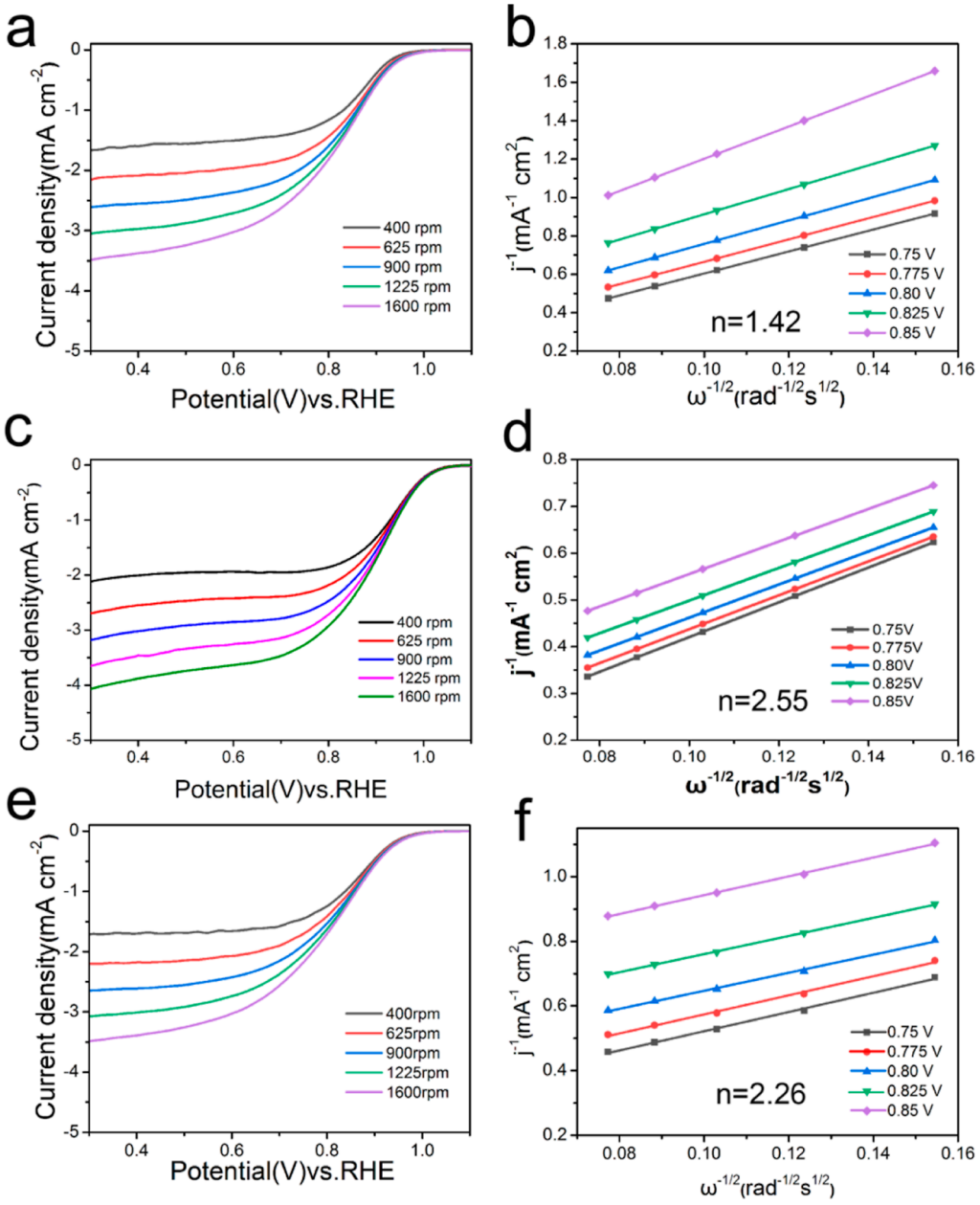

Figure 6. LSV and Koutecky–Levich plots of (a,b) Pd/C_{H_2}, (c,d) Pd/C_M, and (e,f) Pd/C_{H_2+M} at 0.75–0.85 V.

relatively close. As shown in Figure 4b and Table 2, the ECSAs of Pd/C_{H_2}, Pd/C_M, and Pd/C_{H_2+M} were calculated to be 24.39, 43.97, and 34.53 $m^2\ g^{-1}$, respectively. Obviously, Pd/C_M displays the highest ECSAs. This indicates that the unit mass of Pd in Pd/C_M has the most available active sites. This can be attributed to the small size and uniform distribution of the nanoparticles in Pd/C_M. It is worth mentioning that a larger ECSAs is beneficial to improve the interfacial charge transfer and mass diffusion rate and ultimately improve the catalytic activity.

The kinetic current density (j_k), mass activity (MA), and specific activity (SA) can be calculated by the following equation

$$1/j = 1/j_k + 1/j_d$$

where j is the measured current density and j_d is the measured limiting current.[15]

$$MA = j_k / Pd_{loud}$$

$$SA = MA/ECSA$$

It is worth noting that the MA value of the Pd/C_M catalyst is 0.31 A mg^{-1}, which is much higher than that of Pd/C_{H_2} (0.06 A mg^{-1}) and Pd/C_{H_2+M} (0.13 A mg^{-1}) (see Figure 5). Researchers believe that MA, SA, and ECSA are indicators to describe the performance of catalysts from different dimensions. The US Department of Energy proposes using MA as the final evaluation indicator. A higher MA means that less Pd loading is required to maintain battery operation.[16] Pd/C_M achieves an electrochemical activity close to that of high-palladium-loaded catalysts through particle size control at the lowest palladium loading. Therefore, from the comprehensive index, it can be considered that the effect of bioreduction treatment is better. However, Pd/C_{H_2+M} exhibited the worst

https://doi.org/10.1021/acsomega.3c05765
ACS Omega 2023, 8, 47616–47622

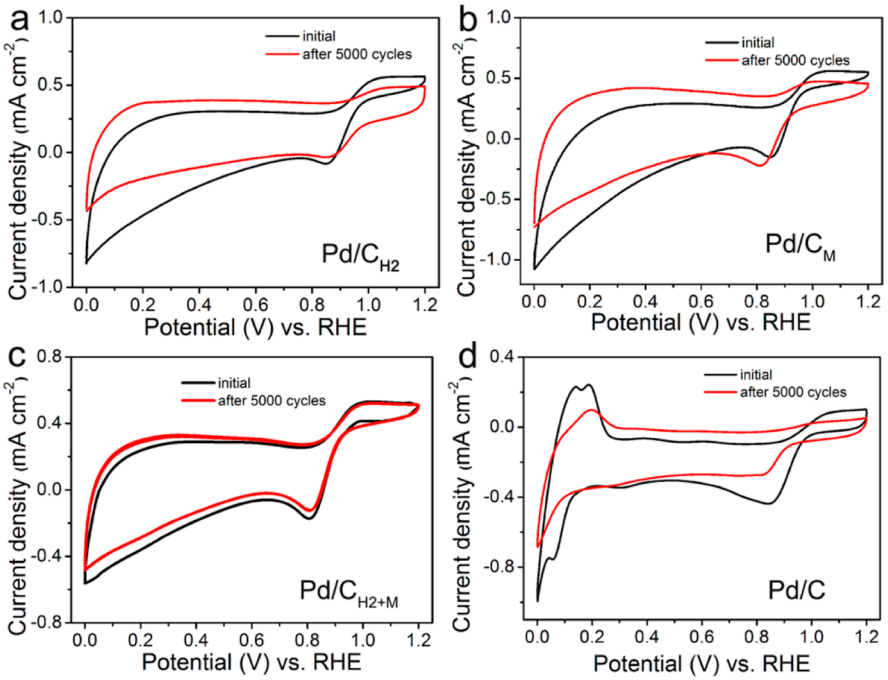

Figure 7. CV curves of (a) Pd/C$_{H_2}$, (b) Pd/C$_M$, (c) Pd/C$_{H_2+M}$, and (d) Pd/C before and after 5000 potential cycles.

performance due to low palladium adsorption under anaerobic conditions and severe agglomeration of palladium particles after two reductions.

Figure 6 shows the LSV and K−L curves of the prepared samples. It can be seen that the electron transfer numbers of Pd/C$_{H_2}$, Pd/C$_M$, and Pd/C$_{H_2+M}$ are 1.42, 2.27, and 1.76, respectively. This is due to differences in the palladium content, particle size, and valence distribution. The bio-reduction process of Pd/C$_M$ was carried out in an anaerobic environment, and the adsorption capacity and reduction rate of palladium ions by Shewanella were low in an anaerobic environment. Low loading palladium (6.63%) and low Pd(0) (35.72%) are not conducive to the electrochemical reaction of the catalyst. However, Pd/C$_M$ avoids the agglomeration of palladium particles under an H_2/Ar atmosphere, so the Pd NPs are the smallest (6.12 nm), which improves the electrochemical performance to a certain extent.

In addition, the electron transfer numbers were calculated through the K−L curve. Compared with the two-electron pathway, the four-electron pathway can provide more power for the fuel cell. By calculating the K−L curve slopes of Pd/C$_{H_2}$, Pd/C$_M$ and Pd/C$_{H_2+M}$ catalysts at 0.75−0.85 V, the average electron transfer numbers are calculated to be 1.42, 2.27, and 1.76, respectively. The Pd/C$_{H_2}$ and Pd/C$_{H_2+M}$ is a two-electron reaction, but Pd/C$_M$ is a mixed electron transfer path of two electrons and four electrons. It can be seen that Pd/C$_M$ has the best catalytic effect in comparison.

One of the most important indicators for evaluating catalyst performance is catalyst stability. The accelerated durability test (ADT) was performed to evaluate the stability. Comparing the CV curves before and after the ADT test (as shown in Figure 7), it was found that the oxygen reduction peaks of Pd/C$_{H_2}$ and Pd/C$_{H_2+M}$ hardly changed, while the oxygen reduction peak of Pd/C$_M$ shifted to the negative direction by 25 mV, but it was still better than that of the commercial Pd/C. In addition, the integral area of the H region of the catalyst decreased, and commercial Pd/C decreased the most. This shows that the durability of the Pd/C catalyst synthesized by the microbial method is higher than that of commercial Pd/C.

4. CONCLUSIONS

In this work, Pd/C catalysts were prepared by different reduction methods using *S. oneidensis* MR-1 as the adsorption matrix. The results show that the reduction method has a great influence on the particle size of palladium. The average particle size of Pd NPs in Pd/C$_{H_2}$, Pd/C$_M$, and Pd/C$_{H_2+M}$ is 17.85, 5.91, and 24.13 nm, respectively. The particle size of Pd NPs in Pd/C$_{H_2+M}$ is the largest, which is due to the smaller palladium particles that have been formed after reduction under anaerobic conditions and will further aggregate and grow in H_2. The particle size of Pd/C$_M$ is the smallest, because it is directly reduced by the microbial redox system, which avoids the migration and agglomeration of palladium atoms under the condition of H_2. In addition, the MA of the Pd/C$_M$ catalyst is 0.31 A mg^{-1}, which is much higher than that of Pd/C$_{H_2}$ (0.06 A mg^{-1}) and Pd/C$_{H_2+M}$ (0.13 A mg^{-1}). The higher MA means that less Pd loading is required to maintain battery operation.

■ ASSOCIATED CONTENT

Supporting Information

The Supporting Information is available free of charge at https://pubs.acs.org/doi/10.1021/acsomega.3c05765.

Detailed electrochemical measurements (PDF)

■ AUTHOR INFORMATION

Corresponding Authors

Xiaoting Deng − *College of Food and Chemical Engineering, Shaoyang University, Shaoyang 422000, China;* orcid.org/0000-0003-0741-3513; Email: xiaotingdeng@126.com

https://doi.org/10.1021/acsomega.3c05765
ACS Omega 2023, 8, 47616−47622

Yili Liang − *School of Minerals Processing and Bioengineering, Central South University, Changsha 410083, PR China*; Email: liangyili6@csu.edu.cn

Authors

Min Lao − *College of Food and Chemical Engineering, Shaoyang University, Shaoyang 422000, China*

Jingwen Huang − *School of Minerals Processing and Bioengineering, Central South University, Changsha 410083, PR China*

Pan Wang − *Changsha Aerospace School, Changsha 410083, China*

Shaofeng Yin − *College of Food and Chemical Engineering, Shaoyang University, Shaoyang 422000, China*

Complete contact information is available at: https://pubs.acs.org/10.1021/acsomega.3c05765

Notes

The authors declare no competing financial interest.

■ ACKNOWLEDGMENTS

The authors gratefully acknowledge financial support from the Foshan Science and Technology Innovation Project (1920001004360), Hunan Provincial Natural Science Foundation of China (2022JJ50171), and Shaoyang University-Hunan Yuxin Pharmaceutical Co., Ltd. school-enterprise cooperation innovation.

■ REFERENCES

(1) Quinson, J.; Kunz, S.; Arenz, M. Surfactant-Free Colloidal Syntheses of Precious Metal Nanoparticles for Improved Catalysts. *ACS Catal.* **2023**, *13* (7), 4903−4937.

(2) (a) Zhou, M.; Wang, H.; Zhang, L.; Li, C.; Kumbhar, A.; Abruña, H. D.; Fang, J. Facet Impact of $CuMn_2O_4$ Spinel Nanocatalysts on Enhancement of the Oxygen Reduction Reaction in Alkaline Media. *ACS Catal.* **2022**, *12* (21), 13663−13670. (b) Li, J.; Xia, W.; Tang, J.; Gao, Y.; Jiang, C.; Jia, Y.; Chen, T.; Hou, Z.; Qi, R.; Jiang, D.; Asahi, T.; Xu, X.; Wang, T.; He, J.; Yamauchi, Y. Metal-Organic Framework-Derived Graphene Mesh: a Robust Scaffold for Highly Exposed Fe-N_4 Active Sites toward an Excellent Oxygen Reduction Catalyst in Acid Media. *J. Am. Chem. Soc.* **2022**, *144* (21), 9280−9291.

(3) (a) Liu, J.; Li, L.; Li, J.; Lin, W.; Wang, H.; Zhao, H.; Chen, X.; Zhang, J.; Yang, W. Lattice-strained Pt nanoparticles anchored on petroleum vacuum residue derived N-doped porous carbon as highly active and durable cathode catalysts for PEMFCs. *Int. J. Hydrogen Energy* **2023**, *48* (66), 25720−25729. (b) Liu, W.; Chen, Q.; Zhang, F.; Xu, D.; Li, X. Atomic metal, N, S co-doped 3D porous nanocarbons: Highly efficient catalysts for HT-PEMFC. *Int. J. Hydrogen Energy* **2021**, *46* (24), 13180−13189.

(4) Zhang, S.; Zhou, H.; Liao, H.; Tan, P.; Tian, W.; Pan, J. Microbial synthesis of efficient palladium electrocatalyst with high loadings for oxygen reduction reaction in acidic medium. *J. Colloid Interface Sci.* **2022**, *611*, 161−171.

(5) Yan, J.; Huang, Y.; Zhang, Y.; Peng, W.; Xia, S.; Yu, J.; Ding, B. Facile Synthesis of Bimetallic Fluoride Heterojunctions on Defect-Enriched Porous Carbon Nanofibers for Efficient ORR Catalysts. *Nano Lett.* **2021**, *21* (6), 2618−2624.

(6) (a) Lin, L.; Yu, Q.; Peng, M.; Li, A.; Yao, S.; Tian, S.; Liu, X.; Li, A.; Jiang, Z.; Gao, R.; Han, X.; Li, Y.-w.; Wen, X.-d.; Zhou, W.; Ma, D. Atomically Dispersed Ni/α-MoC Catalyst for Hydrogen Production from Methanol/Water. *J. Am. Chem. Soc.* **2021**, *143* (1), 309−317. (b) Peng, M.; Dong, C.; Gao, R.; Xiao, D.; Liu, H.; Ma, D. Fully Exposed Cluster Catalyst (FECC): Toward Rich Surface Sites and Full Atom Utilization Efficiency. *ACS Cent. Sci.* **2021**, *7* (2), 262−273.

(7) Moliner, M.; Gabay, J. E.; Kliewer, C. E.; Carr, R. T.; Guzman, J.; Casty, G. L.; Serna, P.; Corma, A. Reversible Transformation of Pt Nanoparticles into Single Atoms inside High-Silica Chabazite Zeolite. *J. Am. Chem. Soc.* **2016**, *138* (48), 15743−15750.

(8) Yang, Y.; Waterhouse, G. I. N.; Chen, Y.; Sun-Waterhouse, D.; Li, D. Microbial-enabled green biosynthesis of nanomaterials: Current status and future prospects. *Biotechnol. Adv.* **2022**, *55*, 107914.

(9) Li, X.; Zhou, Y.; Li, L.; Wang, T.; Wang, B.; Che, R.; Zhai, Y.; Zhang, J.; Li, W. Metal selenide nanomaterials for biomedical applications. *Colloids Surf., B* **2023**, *225*, 113220.

(10) (a) Hou, Y.-N.; Sun, S.-Y.; Yang, Z.-N.; Yun, H.; Zhu, T.-t.; Ma, J.-F.; Han, J.-L.; Wang, A.-J.; Cheng, H.-Y. Shewanella oneidensis MR-1 self-assembled Pd-cells-rGO conductive composite for enhancing electrocatalysis. *Environ. Res.* **2020**, *184*, 109317. (b) Yang, J.; Ju, P.; Dong, X.; Duan, J.; Xiao, H.; Tang, X.; Zhai, X.; Hou, B. Green synthesis of functional metallic nanoparticles by dissimilatory metal-reducing bacteria "Shewanella": A comprehensive review. *J. Mater. Sci. Technol.* **2023**, *158*, 63−76.

(11) Xu, A.; Fan, S.; Meng, T.; Zhang, R.; Zhang, Y.; Pan, S.; Zhang, Y. Catalytic ozonation with biogenic Fe-Mn-Co oxides: Biosynthesis protocol and catalytic performance. *Appl. Catal., B* **2022**, *318*, 121833.

(12) Sun, M.; Xie, Z.; Li, Z.; Deng, X.; Huang, Q.; Li, Z. Electrospun iron and nitrogen co-containing porous carbon nanofibers as high-efficiency electrocatalysts for oxygen reduction reaction. *Int. J. Hydrogen Energy* **2019**, *44* (45), 24617−24627.

(13) Li, G.; Sheng, K.; Lei, Y.; Yang, J.; Chen, Y.; Guo, X.; Chen, G.; Chang, B.; Wu, T.; Wang, X. Facile synthesis of Fe_3C-dominated Fe/Fe_3C/$FeN_{0.0324}$ multiphase nanocrystals embedded in nitrogen-modified graphitized carbon as efficient pH-universal catalyst for oxygen reduction reaction and zinc-air battery. *Chem. Eng. J.* **2023**, *451*, 138823.

(14) Li, Q.; Zhang, S.; Xuan, W.; Zhou, H.; Tian, W.; Deng, X.; Huang, J.; Xie, Z.; Liu, F.; Liu, X.; Liang, Y. Microbial synthesis of highly dispersed nano-Pd electrocatalyst for oxygen reduction reaction. *Int. J. Hydrogen Energy* **2021**, *46* (53), 26886−26896.

(15) Wang, X.; Guo, L.; Xie, Z.; Peng, X.; Yu, X.; Yang, X.; Lu, Z.; Zhang, X.; Li, L. Coordination environment engineering of graphene-supported single/dual-Pd-site catalysts improves the electrocatalytic ORR activity. *Appl. Surf. Sci.* **2022**, *606*, 154749.

(16) Xia, Y.-F.; Guo, P.; Li, J.-Z.; Zhao, L.; Sui, X.-L.; Wang, Y.; Wang, Z.-B. How to appropriately assess the oxygen reduction reaction activity of platinum group metal catalysts with rotating disk electrode. *iScience* **2021**, *24* (9), 103024.

■ NOTE ADDED AFTER ASAP PUBLICATION

This paper originally published ASAP on December 1, 2023. Figure 2 was corrected, and a new version reposted December 4, 2023.